J. Fluid Mech. (1993), *vol.* 257, *pp.* 289–309

Boiling in a porous layer heated from below: effects of natural convection and a moving liquid/two-phase interface

By P. S. RAMESH† AND K. E. TORRANCE

Sibley School of Mechanical and Aerospace Engineering, Cornell University, Ithaca, NY 14853, USA

(Received 18 December 1991 and in revised form 25 May 1993)

Boiling and natural-convection processes in a horizontal, fluid-saturated porous layer are investigated. The layer is heated uniformly from below and is cooled from above. Volumetric cooling is also allowed. The thermodynamic structure consists of a liquid region overlying a two-phase region. Numerical techniques are used to solve the transient, two-dimensional equations in the liquid and two-phase regions, and at the phase-change interface. A parametric study is carried out in terms of the liquid-phase Rayleigh number (Ra) and the non-dimensional bottom heat flux (Q_b). Three solution regimes are observed: conduction-dominated at low Ra, convection-dominated at intermediate Ra, and oscillatory convection at high Ra. In the convection-dominated regime, transitions to multiple cell patterns are observed as Q_b is increased. Oscillatory convection appears to be triggered by asymmetric disturbances in the system. The effects of initial conditions and the stability of the solutions to perturbations are also investigated. The heat transfer correlations and qualitative flow patterns are in agreement with experiments.

1. Introduction

Boiling and natural convection represent two important heat transport mechanisms. In many problems, such as geothermal reservoirs, heat transfer by boiling and natural convection occur simultaneously, and their interactions are of fundamental as well as practical interest. The objective of this paper is to present a systematic study of boiling and natural convection in a fluid-saturated porous medium with an internal interface between the boiling and non-boiling zones. The present study is a numerical one, and it complements several experimental investigations previously reported in the literature.

Heat transport phenomena in porous media have been receiving increased attention in the last decade or so. While much of the literature pertains to single-phase thermal convection, two-phase convection is probably the more dominant mode of heat transfer in geothermal systems. Studies on boiling in porous media have been mainly experimental, and theoretical studies have been restricted to one-dimensional geometries. Torrance (1983) presents a review of laboratory experiments on boiling in porous media, and Cheng (1978) and Bjornsson & Stefansson (1987) discuss the geothermal aspects.

Experimental studies have considered porous beds heated from below and cooled from above. The geometries have varied from two-dimensional Hele-Shaw cells (Sondergeld & Turcotte 1978; Tewari 1982; Echaniz 1984) to cylindrical (Bau &

† Current address: Xerox Corp., Design Research Institute, Engineering and Theory Center, Cornell University, Ithaca, NY 14853, USA.

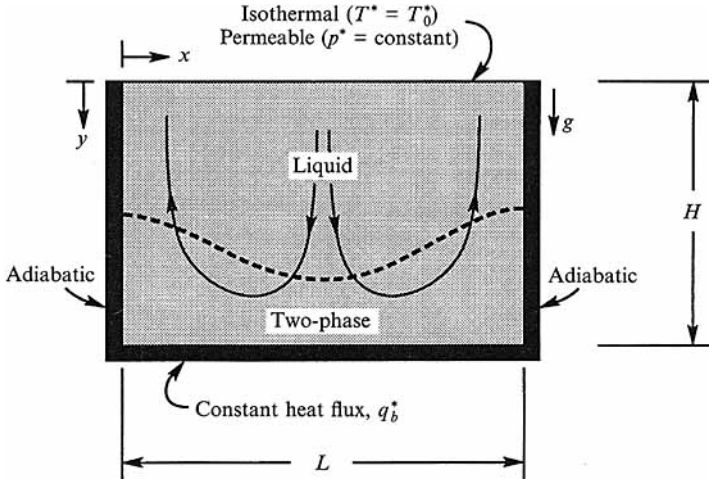

FIGURE 1. Schematic of a two-layer phase structure in a fluid-saturated porous medium heated from below and cooled from above. Example liquid-phase streamlines are shown.

Torrance 1982*a*, *b*) and three-dimensional box geometries (Sondergeld & Turcotte 1977). In all cases, the preferred phase structure is that of a liquid region overlying a two-phase region (figure 1). The underlying two-phase region is liquid dominated, essentially isothermal, and heat is transported by liquid–vapour counterpercolation.

Several hydrodynamic regimes have been observed in the above-mentioned experiments. For low-permeability porous beds, the overlying liquid region is conduction dominated, and experiments agree well with one-dimensional models (Bau & Torrance 1982*a*). For intermediate-permeability porous beds, the liquid region becomes convective, interacts with the underlying two-phase region, and multi-dimensional flows result. Two scenarios are possible. In the first scenario, thermal convection in the liquid region starts immediately or soon after the onset of boiling (Sondergeld & Turcotte 1977). Sondergeld & Turcotte (1977) concluded that a phase-change mechanism is responsible for driving the convection. In the second scenario, the convection starts before the onset of boiling (Tewari 1982; Bau & Torrance 1982*b*; Echaniz 1984). Visualization experiments (Tewari 1982; Sondergeld & Turcotte 1978) in a Hele-Shaw geometry clearly showed the liquid-region streaklines penetrating the two-phase region, and considerable interaction existed between the two regions. The phase-change interface between the liquid and two-phase regions is raised in the region of upwelling of the hot fluid, and depressed in the region of downwelling of the cold fluid (as sketched in figure 1).

For high-permeability beds, the steady behaviour is replaced by an oscillatory regime (Tewari 1982; Echaniz 1984). This oscillatory regime is characterized by time-dependent fluctuations of the convective cell pattern. Echaniz (1984) carried out a detailed study of the oscillations using a network of thermocouples and computerized data acquisition. He concluded that the oscillations are caused by thermals (pairs of small vortices) which originate at the heating surface. The thermals are born where the cold fluid descends, and they grow and disappear either at the top boundary or in the two-phase region. Similar mechanisms have been proposed for oscillatory convection in the absence of boiling (Horne & Caltagirone 1980). As the heat flux is increased, the period of oscillations becomes shorter. In the laboratory experiments, these periods varied from a few hours at low heat fluxes to a few minutes at high fluxes.

In an effort to understand the interaction between boiling and natural convection phenomena, Ramesh & Torrance (1990*a*) recently carried out a linear stability analysis of boiling in porous media using the preferred two-layer phase structure with a conduction-dominated liquid region as the rest-state solution. They argued that boiling in porous media heated from below is governed primarily by two parameters: the liquid-phase Rayleigh number based on the temperature difference across the porous bed (Ra), and the dimensionless heat flux at the bottom (Q_b). They showed that for liquid-dominated systems, the critical Rayleigh number is lowered by the presence of a two-phase region thereby enabling thermal convection in the liquid region to set in after the onset of boiling. They used a stability diagram in Ra–Q_b parameter space to provide a qualitative understanding of the laboratory experiments. In a related study, Ramesh (1988) analysed the energies of perturbations in such a system and showed that the convective instability may be produced by both thermal buoyancy and phase-change effects.

This paper presents a detailed numerical study of natural convection with boiling in a fluid-saturated porous layer. A two-dimensional rectangular porous bed with properties representative of laboratory experiments is used. The objective of the study is to obtain finite-amplitude solutions of liquid-region convection in the presence of boiling. Experiments on boiling in porous media clearly display a wide range of behaviour. We seek to understand the transitions between the conduction-dominated solutions at low permeabilities and the steady convection-dominated solutions and oscillatory convection solutions at higher permeabilities.

In the following section (§2), the governing equations in the liquid (non-boiling) and two-phase (boiling) regions are presented, together with the compatibility conditions at the interface between the regions. These equations are solved numerically using the approach proposed in Ramesh & Torrance (1990*b*). A parametric study is carried out in Ra–Q_b parameter space to explore the range of possible solutions (§3). The effects of initial conditions, the stability of the solutions to perturbations, and comparisons with experiments and linear stability analysis are reported.

2. Mathematical formulation

We consider a porous domain bounded by two horizontal parallel planes which are separated by a distance H as sketched in figure 1. We assume a finite lateral dimension L and two-dimensional motion in the (x, y)-plane. We further assume the porous layer to be uniform, isotropic and fully saturated with fluid.

2.1. *Governing equations*

The thermodynamic structure of the porous medium after the onset of boiling consists of a liquid region overlying a two-phase region. The Boussinesq approximation is used to account for buoyancy effects in the liquid region. The two-phase region is taken to be isothermal at the boiling temperature (T^*_{sat}).

The equations are made non-dimensional using the following reference quantities: length, H; time, H^2/α_l where α_l is the thermal diffusion coefficient of the liquid-saturated porous medium; and temperature, $T = (T^* - T^*_0)/(T^*_{sat} - T^*_0)$ where T^*_0 is the temperature of the top boundary. The governing equations in the liquid and two-phase regions in dimensionless form are:

liquid

$$\nabla \cdot v_l = 0 \quad \text{(continuity)}, \tag{1}$$

$$\boldsymbol{v}_l = -\nabla p - Ra\, T \boldsymbol{e}_y \quad \text{(Darcy's eq.)} \tag{2}$$

$$\beta_1 \frac{\partial T}{\partial t} + \boldsymbol{v}_l \cdot \nabla T = \nabla^2 T - Bi\, T \quad \text{(energy)}; \tag{3}$$

two-phase

$$\beta_2 \frac{\partial S}{\partial t} + \nabla \cdot (\boldsymbol{v}_l + \bar{\rho}_v \boldsymbol{v}_v) = 0 \quad \text{(continuity)}, \tag{4}$$

$$\boldsymbol{v}_l = -k_{rl}(\nabla p + Ra\, \boldsymbol{e}_y) \quad \text{(Darcy's eq. for liquid)}, \tag{5}$$

$$\boldsymbol{v}_v = -k_{rv} \bar{\mu}_l (\nabla p + Ra_{2\phi}\, \boldsymbol{e}_y) \quad \text{(Darcy's eq. for vapour)}, \tag{6}$$

$$\phi \bar{\rho}_v \lambda \frac{\partial}{\partial t}(1-S) + \nabla \cdot (\bar{\rho}_v \lambda \boldsymbol{v}_v) = -Bi \quad \text{(energy)}; \tag{7}$$

where the quantities T, p, $\boldsymbol{v}$ and S are the temperature, pressure, velocity vector and liquid saturation, respectively; ϕ denotes the porosity of the layer; the subscripts l, v, and s represent liquid, vapour, and porous medium, respectively; $\boldsymbol{e}_y$ is the unit vector in y which is assumed positive in the direction of the gravity vector.

Ra is the liquid-phase Rayleigh number given by

$$Ra = \frac{KHg\beta_l (T^*_{sat} - T^*_0)}{\nu_l \alpha_l}, \tag{8}$$

where K is the permeability of the porous layer, g is the acceleration due to gravity, β_l is the liquid thermal expansion coefficient, $(T^*_{sat} - T^*_0)$ represents the difference between the boiling temperature (T^*_{sat}) and the temperature of the top boundary (T^*_0), and ν_l denotes the kinematic viscosity of the liquid phase. $Ra_{2\phi}$ is the two-phase Rayleigh number based on the density difference between the phases given by

$$Ra_{2\phi} = \frac{KHg(1-\bar{\rho}_v)}{\nu_l \alpha_l}, \tag{9}$$

where $\bar{\rho}_v = \rho_v/\rho_l$ and ρ denotes the density. We note that the two Rayleigh numbers are related by a density ratio parameter, $\gamma = Ra/Ra_{2\phi}$, which is the ratio of the maximum density change in the liquid region to the density difference between phases in the two-phase region. γ involves physical properties and boundary temperatures. If these are known, Ra and $Ra_{2\phi}$ are not independent, but are related by $Ra = Ra_{2\phi}\gamma$. We also note that for a given working fluid, Ra may be used as a measure of the permeability of the porous layer.

Bi is a volumetric heat loss parameter. It accounts for thermal losses through the front and back walls of a Hele-Shaw type convection cell. Such losses are proportional to the temperature difference between the porous bed and the surrounding ambient medium. For a Hele-Shaw geometry,

$$Bi = \frac{2hH^2}{k_e \Delta}, \tag{10}$$

where h is the heat transfer coefficient from the bed to the ambient, k_e is the effective thermal conductivity of the porous matrix, and Δ is an effective front-to-back thickness of the Hele-Shaw cell. The ambient temperature is assumed to be T^*_0.

Additional parameters appearing in equations (1)–(7) are: λ, a latent heat parameter, $= h_{fg}/(C_l(T^*_{sat}-T^*_0))$ where h_{fg} is the latent heat of vaporization and C is the specific heat at constant pressure; $\beta_1 = ((1-\phi)\rho_s C_s+\phi\rho_l C_l)/(\rho_l C_l)$ is a ratio of heat capacities; $\beta_2 = \phi(1-\bar{\rho}_v)$; and $\bar{\mu}_l = \mu_l/\mu_v$ is the ratio of viscosities (μ). k_{rl} and k_{rv} are the relative permeabilities for the liquid and vapour phases in the two-phase region which account for the drag due to the presence of the other phase. k_{rl} and k_{rv} are typically expressed as functions of the saturation (Torrance 1983), although linear forms are assumed here.

Note in (5) and (6), that the liquid and vapour phases in the two-phase region are locally taken to be at the same pressure, p. This follows when the mean radius of curvature of the interfaces separating the phases (at the pore level) is large, and the capillary pressure difference may be neglected. Thus, in (5) and (6), the flow of each phase is driven by the difference between ∇p and the hydrostatic gradient for each phase. Capillary pressure effects can arise for very fine-grain porous media, or when wicking action (and not gravity) is important for the movement of the liquid phase. For simplicity, capillary pressure effects will be neglected in the present analysis.

The interface between the liquid and two-phase regions is represented functionally by $y = \delta(x,t)$. We assume that δ is continuous and differentiable. The following compatibility conditions are prescribed at the interface, $\delta(x,t)$:

$$p^+ = p^- \quad \text{(pressure is continuous across the interface)}, \tag{11}$$

$$T^- = 1 \quad \text{(the interface is at the phase change temperature)}, \tag{12}$$

$$(\boldsymbol{v}_l^- - (\boldsymbol{v}_l^+ + \bar{\rho}_v \boldsymbol{v}_v^+) - \alpha_1 \boldsymbol{v}_i)\cdot \boldsymbol{n} = 0 \quad \text{(mass balance)}, \tag{13}$$

$$(\nabla T^- + \bar{\rho}_v \lambda \boldsymbol{v}_v^+ - \alpha_2 \boldsymbol{v}_i)\cdot \boldsymbol{n} = 0 \quad \text{(energy balance)}, \tag{14}$$

where $\alpha_1 = \phi(1-\bar{\rho}_v)(1-S)$ and $\alpha_2 = \phi\bar{\rho}_v\lambda(1-S)$. $\boldsymbol{v}_i$ denotes the local velocity of the interface, and $\boldsymbol{n}$ the unit vector normal to the interface. The superscripts $-$ and $+$ represent the liquid and the two-phase sides of the interface, respectively.

2.2. *Boundary conditions*

The upper boundary is permeable (see figure 1) and therefore allows for non-zero normal velocities. This boundary is modelled as a constant-pressure surface ($p = 0$). Physically, this allows natural discharge and recharge of fluid at the upper boundary, as would occur if the upper boundary were overlain by a liquid reservoir. The temperature at the upper boundary is maintained at ambient temperature ($T = 0$). The bottom boundary is treated as impermeable with a uniform heat flux Q_b prescribed upon it, with Q_b defined as

$$Q_b = \frac{q_b^* H}{k_e(T^*_{sat}-T^*_0)}, \tag{15}$$

where q_b^* is the dimensional heat flux at the bottom boundary. Note that $Q_b = 1$ represents the maximum conduction flux across a liquid-saturated porous layer of height H and conductivity k_e before the onset of boiling (for the case when $Bi = 0$). When a two-phase region is in contact with the bottom boundary, the impermeability condition implies zero net mass flux, i.e. $(\boldsymbol{v}_l+\bar{\rho}_v\boldsymbol{v}_v)\cdot\boldsymbol{n} = 0$; and the thermal boundary condition implies $\bar{\rho}_v\lambda\boldsymbol{v}_v\cdot\boldsymbol{n} = Q_b$. Therefore, the two-phase region supports non-zero fluxes of liquid and vapour at the bottom boundary which are each equal in magnitude to the rate of evaporation. The lateral boundaries at $x = 0$ and AR are impermeable and adiabatic. Heat losses from the front and back boundaries (i.e. the z-boundaries of a Hele-Shaw cell) are modelled with the Bi term.

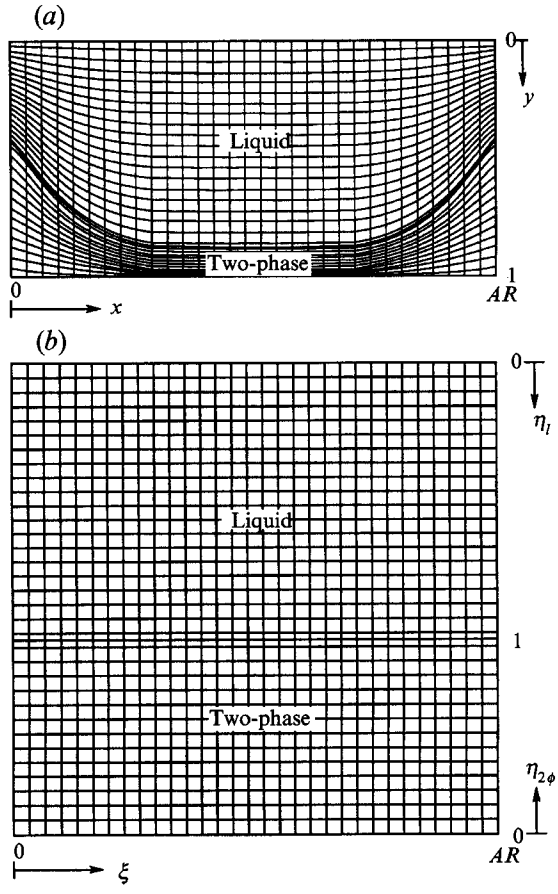

FIGURE 2. Typical computational grid in (*a*) the physical domain and (*b*) the transformed domain.

2.3. *Numerical method*

The numerical scheme is based on a fully implicit finite-difference control volume method. The scheme solves the coupled flow and heat transfer equations for the liquid region, two-phase region, and the interface. The Landau coordinate transformation ($\xi = x, \eta_l = y/\delta$ in the liquid region, and $\eta_{2\phi} = (1-y)/(1-\delta)$ in the two-phase region) is used to fix the interface in (ξ, η)-coordinates at $\eta = 1$ (see figure 2). The equations are discretized and solved in the transformed spatial domain.

At each time step, the scheme advances the interface using the local energy balance (equation (14)). Subsequently, the pressure, saturation (in the two-phase region) and temperature (in the liquid region) are advanced. Iteration is performed until the position of the interface converges at the new time level before advancing to the next time level. The implicit nature of the solution, including the implicit movement of the interface, allows stable time integration. A detailed description of the numerical algorithm and its accuracy and convergence properties is given in Ramesh & Torrance (1990*b*).

An important aspect of this study is the stability of the conduction and finite-amplitude convection solutions to symmetric and asymmetric disturbances. Traditional wisdom is that higher-order spatial schemes (e.g. fourth-order) are required to resolve oscillatory flows (Gary & Kassoy 1981), as against second-order accuracy required to

resolve steady convection flows. The present numerical scheme is only second-order accurate (Ramesh & Torrance 1990*b*) and to incorporate a fourth-order scheme within the framework of the present problem would be very expensive computationally, and is beyond the scope of this study. However, an important feature of the present numerical scheme is the accurate solution of the Poisson equation for pressure using a pre-conditioned conjugate gradient algorithm. Iterative schemes such as successive over-relaxation which involve sweeps along specific spatial directions are unsuitable for stability studies because they can introduce spatial bias in the temperature fields which can affect the preferred convective solution. The conjugate gradient algorithm on the other hand appears to be free from any spatial bias and can be used reliably to study the stability of solutions to different wavelength disturbances. The numerical scheme was benchmarked successfully for several cases involving the onset of convection (single-phase and two-phase convection), and finite-amplitude solutions (for single-phase convection) prior to its use in the present study (Ramesh 1988).

In the present study, the typical run times for steady solutions on an IBM 3090-600E computer varied from 200 CPU seconds on a coarse grid ($16 \times \overline{10+7}$) to 1000 CPU seconds on a fine grid ($32 \times \overline{20+14}$). Oscillatory solutions were comparatively expensive to compute owing to the long periods of oscillations and the large number of time steps needed to follow them. A typical run time for an oscillatory solution on a $24 \times \overline{15+10}$ grid was about 2500 CPU seconds. Note that a $M \times \overline{N_l + N_{2\phi}}$ grid denotes M node points in ξ, N_l node points in η_l, and $N_{2\phi}$ node points in $\eta_{2\phi}$.

3. Results and discussion

The primary parameters of interest are the liquid Rayleigh number Ra and the non-dimensional heat flux at the bottom Q_b. The parameter Bi controls the rest-state conduction solution of the system, which ranges from a linear temperature profile for $Bi = 0$ to an exponential one for $Bi > 0$. Linear stability analyses with zero and non-zero values of Bi have yielded essentially the same qualitative features for the solution regimes (Ramesh & Torrance 1990*a*; Ramesh 1988; see also figure 15 here). For the present study, Bi is assumed to be fixed. To allow some limited comparison with laboratory experiments, an aspect ratio of $L/H = 2$ and a value of $Bi = 8.4$ are assumed.

Representative ranges examined for the Ra and Q_b parameters are $0 \leqslant Ra \leqslant 60$ and $0 \leqslant Q_b \leqslant 12$. The physical property parameters are evaluated using water as the working fluid, $T_0^* = 30$ °C and $T_{sat}^* = 100$ °C (typical of laboratory experiments), liquid and vapour properties evaluated at T_0^* and T_{sat}^*, respectively, and a porous medium consisting of glass beads or silica sand: therefore, $\phi = 0.35$, $\bar{\rho}_v = 0.6068 \times 10^{-3}$, $\bar{\mu}_l = 38.67$, $\rho_s C_s / \rho_l C_l = 0.5820$, $\gamma = 0.03663$ and $\gamma = 7.706$. These values are held fixed. In addition, we choose linear relative permeabilities, $k_{rl} = S$ and $k_{rv} = 1 - S$, and assume the two-phase region to be liquid dominated.

Two types of initial condition are of interest for stability studies. The first is the conduction solution (one-dimensional) for the given set of input parameters (Ra, Q_b) which is perturbed by introducing hot and cold spots (of magnitude 0.001) along $y = 0.5$ in the temperature field. These perturbations generate a weak convective flow of the desired cellular pattern. This initial flow may grow, decay or migrate to an alternate cellular pattern. In the absence of the perturbation, the solution does not depart from the initial condition. (This implies that the numerical scheme itself is relatively noise free, and does not generate flows due to error accumulation.) We consider two types of perturbations: symmetric perturbations (about $x = 1$) which are obtained by

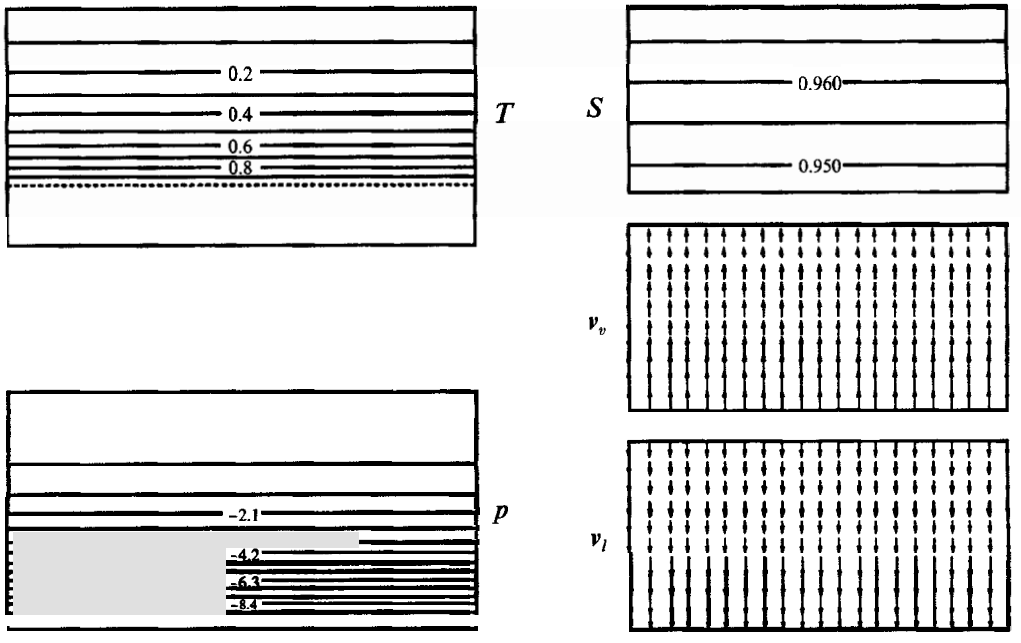

FIGURE 3. Steady-state temperature T and pressure p in a porous layer with a quiescent liquid zone overlying a two-phase zone, $Ra = 20$, $Q_b = 5$. The dashed line denotes the upper boundary of the two-phase zone. On the right-hand side are shown, in transformed coordinates, the saturation S, vapour velocity $\boldsymbol{v}_v$ and liquid velocity $\boldsymbol{v}_l$ in the two-phase zone, with $|\boldsymbol{v}_v|_{max} = |\boldsymbol{v}_l|_{max} = 0.63$.

No.	Ra	Q_b	Grid	Initial condition	Solution regime
A1	20	5	$16\times10\times7$	COND for $Q_b = 3$	III (figure 3)
B1		3	$16\times10\times7$	COND	III (figure 5*a*)
B2		4	$32\times20\times14$	B3	IV (two cells, figure 5*b*)
B3	40	5	$32\times20\times14$	COND	IV (two cells, figure 5*c*)
B4		7	$32\times20\times14$	B3	IV (two cells, figure 5*d*)
B5		10	$32\times20\times14$	B3	IV (two cells, figure 5*e*)
C1		2.5	$32\times20\times14$	COND	II (two cells, figure 6*a*)
C2	50	5	$32\times20\times14$	B3	IV (two cells)
C3		7	$32\times20\times14$	B4	IV (two cells, figure 6*b*)
C4		10	$32\times20\times14$	B5	IV (two cells)
D1		2.5	$32\times20\times14$	C1	II (two cells, figure 7*a*)
D2	60	5	$32\times20\times14$	C2	IV (two cells, figure 7*b*)
D3		7	$32\times20\times14$	C3	IV (four cells, figure 7*c*)
D4		10	$32\times20\times14$	D3	IV (four cells, figure 7*d*)
E1	40	12	$16\times10\times7$	COND	III
E2	40	12	$32\times20\times14$	B5	IV (two cells)
F1	60	7	$24\times15\times10$	COND+ASYM	IV (oscillatory, figures 11, 13)
F2	60	10	$24\times15\times10$	COND+ASYM	IV (oscillatory, figures 12, 14)

TABLE 1. Summary of numerical simulations. COND denotes a one-dimensional conduction solution with symmetric perturbations, and COND+ASYM denotes a one-dimensional conduction solution with asymmetric perturbations. The final column refers to regions shown on figure 15: I denotes a conductive liquid layer; II a convective liquid layer; III a conductive liquid layer overlying a two-phase layer; and IV a convective liquid layer overlying a two-phase layer (flows can be steady or oscillatory).

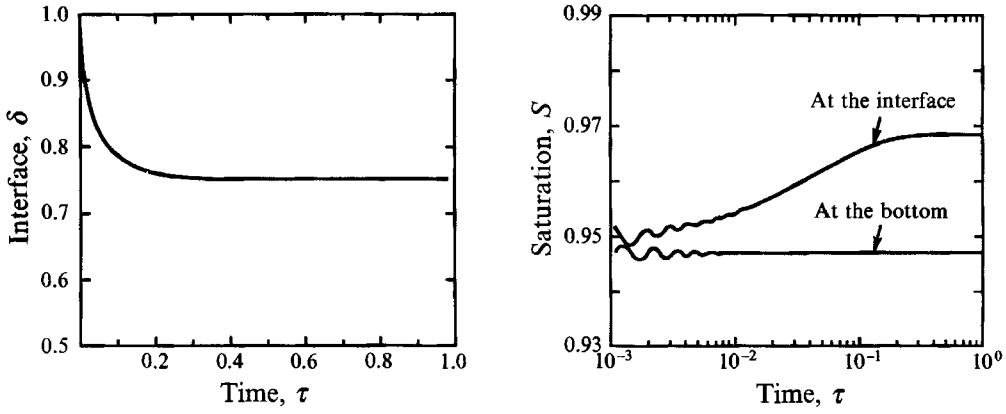

FIGURE 4. Transient evolution of interface position δ and saturation in the two-phase region S corresponding to the conditions of figure 3, $Ra = 20$, $Q_b = 5$. The interface is planar at all times. Initial condition: $Q_b = 3$.

introducing two hot spots along the sides ($x = 0, 2$) and one cold spot in the middle ($x = 1$); and asymmetric perturbations which are obtained by introducing a hot spot at $x = 0$ and a cold spot at $x = 2$. A second type of initial condition used is the converged solution from a different set of input parameters.

A summary of the numerical experiments is given in table 1. Three solution regimes are observed: conduction dominated, steady convection dominated, and oscillatory convection. In some cases the solutions exhibit a dependence on initial conditions and perturbations.

3.1. *Conduction-dominated regime*

Conduction-dominated solutions occur for small Ra (low permeabilities). The steady-state fields (figure 3) indicate one-dimensional behaviour. The liquid and vapour velocity fields in the two-phase region clearly show heat transport due to counterpercolation. There is slightly less vapour at the top of the two-phase region (larger S) than at the bottom owing to vapour condensation due to sidewall heat loss to the ambient (i.e. the Bi term).

The transient evolution of the interface position and the two-phase saturation field due to a step change in bottom heat flux (from $Q_b = 3$ to $Q_b = 5$) are shown in figure 4. The interface is planar at all times, indicating the absence of buoyancy-driven convection in the liquid region. The timescale for saturation transients in the two-phase region is 3 to 4 orders of magnitude smaller than the thermal diffusion timescale for the porous layer (i.e. the reference timescale). The chosen time step ($\Delta t = 10^{-4}$), while it is sufficient to resolve interface movements and other transient fields, is too large to resolve early saturation transients in the two-phase region. The oscillations observed at early times in the saturation profile result from this. The saturation at the bottom of the two-phase region reaches steady state almost instantaneously ($t \approx 10^{-3}$), but the saturation near the top of the two-phase region continues to change owing to the motion of the interface.

3.2. *Steady convection-dominated regime*

The onset of convection takes place when the Rayleigh number exceeds the critical value (Ramesh & Torrance 1990*a*). Convection can set in before or after the onset of boiling.

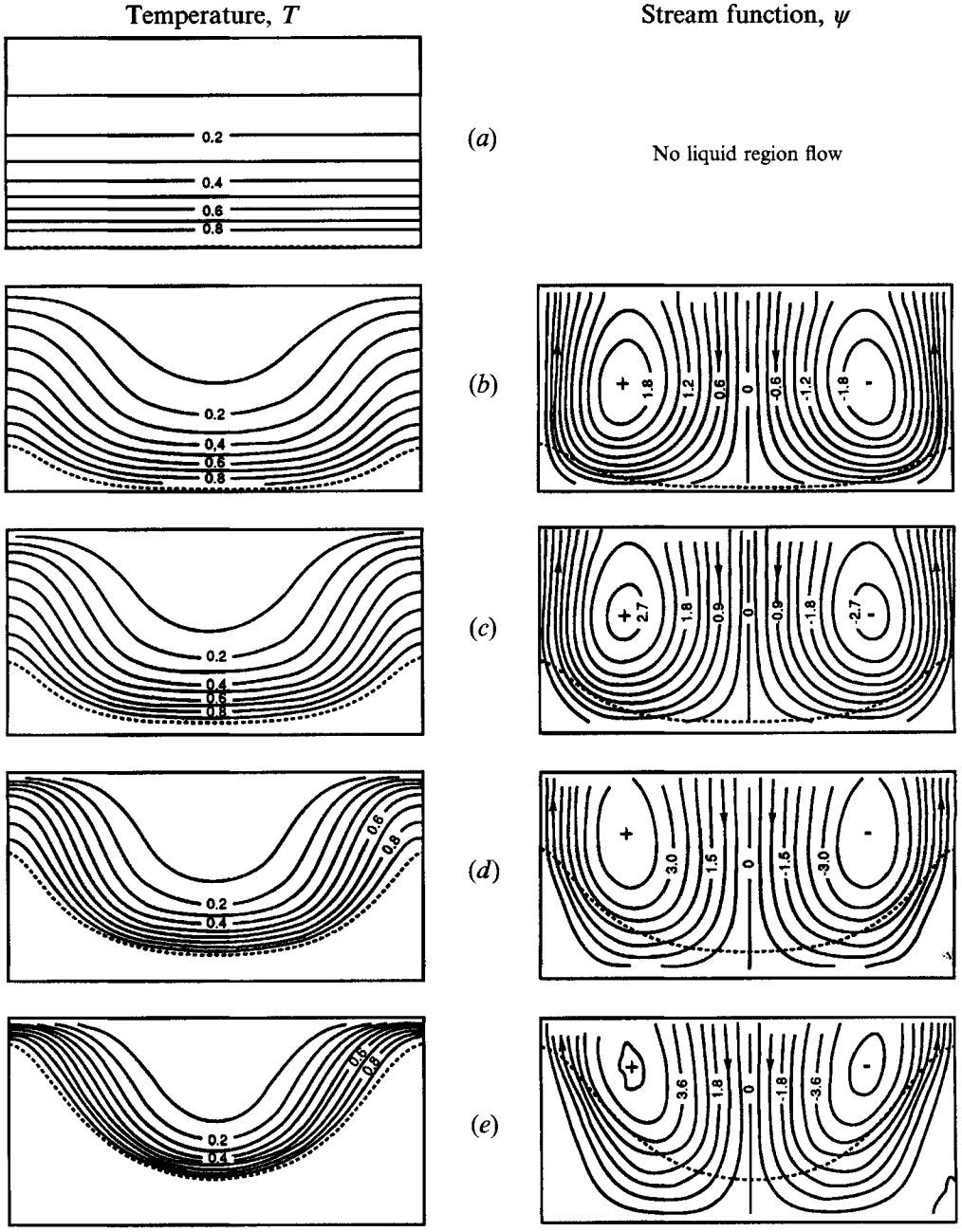

FIGURE 5. Steady state temperature T and stream function ψ for $Ra = 40$ and various heating rates, Q_b: (*a*) $Q_b = 3$, (*b*) 4, (*c*) 5, (*d*) 7 and (*e*) 10. The onset of convection occurs after the onset of boiling.

3.2.1. *Onset of convection after the onset of boiling*

In this regime, the solution is conduction dominated at the onset of boiling (figure 5*a*, $Ra = 40$, $Q_b = 3$), but convection sets in as the bottom heat flux is increased (figure 5*b–e*, $Ra = 40$, $Q_b \geqslant 4$). Note that the stream function (ψ) for the convective solutions is based on $\boldsymbol{v}_l$ in the liquid region, and $\boldsymbol{v}_l + \bar{\rho}_v \boldsymbol{v}_v$ in the two-phase region. The preferred convective mode is two cells. The solution is symmetric about the centre ($x = 1$).

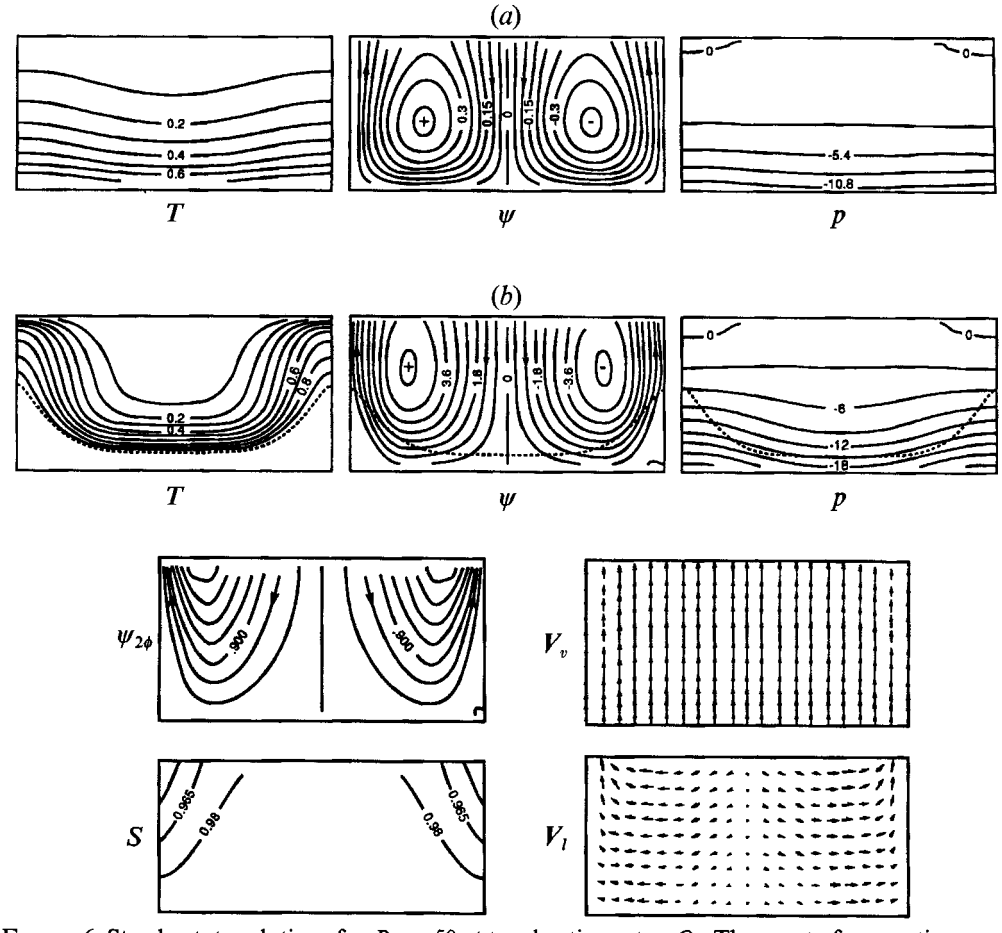

FIGURE 6. Steady-state solutions for $Ra = 50$ at two heating rates, Q_b. The onset of convection occurs before the onset of boiling. (*a*) $Q_b = 2.5$. Convection but no boiling. (*b*) $Q_b = 7$. Convection with boiling. The four lower figures show, in transformed coordinates, $\psi_{2\phi}$, S, v_v and v_l in the two-phase zone, with $|v_v|_{max} = 0.91$ and $|v_l|_{max} = 23.66$ in the two-phase region.

Many qualitative aspects of the experimental results are preserved in the numerical solutions. The interface (dotted line) moves up as the heat flux is increased. The interface is depressed in the middle indicating downflow of the cold fluid, and raised at the sides indicating upflow of the warm fluid. The strength of the circulation ($|\psi|_{max}$) increases with heat flux. The centre of the cell always lies in the liquid region. This is because the buoyancy production term is present in the liquid region, and not in the two-phase region. The liquid velocities are of the order of 10^{-5} m/s, which is consistent with the velocities of streaklines observed in visualization experiments (Sondergeld & Turcotte 1978; Tewari 1982).

3.2.2. *Onset of convection before the onset of boiling*

Results for $Ra = 50$ and 60 are shown in figures 6 and 7, respectively. The single-layer solution before the onset of boiling ($Q_b = 2.5$, figures 6*a*, 7*a*) shows a stable two-cell convection pattern. This pattern is retained after the onset of boiling (figures 6*b*, 7*b*). The pressure contours (figure 6*b*) indicate larger pressure gradients in the two-phase region. Larger pressure gradients also exist near the interface on the liquid side due to the higher temperatures.

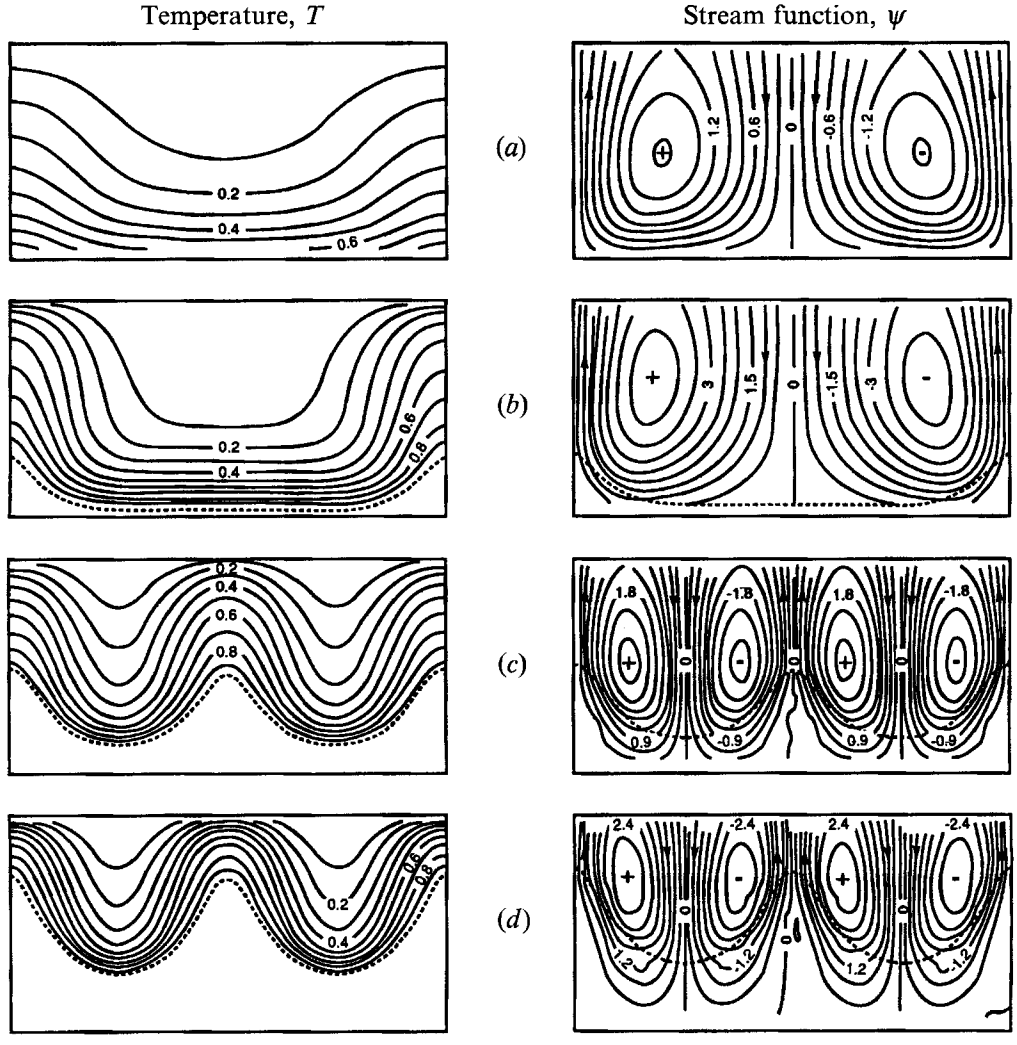

FIGURE 7. Steady-state temperature T and stream function ψ for $Ra = 60$ and various heating rates, Q_b. The onset of convection occurs before the onset of boiling. (*a*) $Q_b = 2.5$, (*b*) 5, (*c*) 7, (*d*) 10.

In the region of downflow (i.e. the middle), the liquid moves slowly but heats up over a relatively short region, which is corroborated by the larger temperature gradient in the middle. The energy balance at the interface (equation (14)) at steady state implies a balance between the energy released by condensation of vapour and the conductive heat flux in the liquid region at the interface. Consequently, the vapour velocities are larger in the middle, and also there is more vapour present in the middle as is evident from the saturation contours (figure 6*b*). The energy for evaporation of the liquid crossing the interface near the middle is provided by the condensation of this excess vapour. In the two-phase region, the liquid velocity field is more or less aligned with the stream function ($\psi_{2\phi}$). Note that $\psi_{2\phi}$ is plotted in the transformed space (ξ, $\eta_{2\phi}$) for greater clarity. There is counterflow of liquid and vapour in the middle, while there is crossflow near the sides. Similar behaviour for liquid and vapour flow in liquid-dominated systems has been observed in Lasseter's calculations (Lasseter 1975).

For $Ra = 60$ (figure 7), a transition from the two-cell structure to a steady four-cell

	Experiments	Present study
Q_{top} for steady convection	$\propto Ra_f^{0.5}$	$\propto Ra_f^{0.6}$
Mean Q_{top} for oscillatory convection	$\propto Ra_f^{0.975}$	$\propto Ra_f^{1.22}$
Time period of oscillation	$\propto Ra_f^{-0.64}$	$\propto Ra_f^{-0.5}$

TABLE 2. Comparison between experiments (Echaniz 1984) and present numerical simulations. ($Ra_f = RaQ_b$).

structure is observed as Q_b is increased from 5 to 7 (figure 7*b*, *c*). All four cells are of approximately the same strength, and the solution is again symmetric about the centre. Tewari (1982) also observed transitions from two to four cells in his experiments as he increased the heat flux. However the stable three-cell solutions observed in Tewari's experiments were not observed in the present numerical simulations. This may be attributed to slight inhomogeneities in the experimental bed leading to non-uniformities of the bottom heating which have not been modelled computationally. It is encouraging, however, to note that the numerical scheme is able to accurately follow the transition from two to four cells.

Transient features of the case $Ra = 50$, $Q_b = 7$ are shown in figures 8 and 9. The steady-state solutions for this case were discussed earlier in connection with figure 6(*b*). The initial condition is the one-dimensional conduction solution with a flat interface. Convection sets in at time ≈ 0.25, and the interface continues to distort as the convection gains in strength (figure 8). The interface moves down, thereby lowering the temperature gradients in the liquid region. It is interesting to note that the interface shape remains symmetric about the centre at all times. This is a consequence of the symmetric perturbations introduced in the initial condition. The heat transfer at the top of the porous bed (Q_{top}) versus time is plotted in figure 9. The onset of convection is indicated by the sudden rise in the heat transfer rate. There is an overshoot of the steady-state interface position and a corresponding overshoot in the value of Q_{top} because the interface motion is rapid compared to the diffusion timescales.

The steady-state heat flux, Q_{top}, for the two-cell solutions is shown in figure 10 as a function of the heat-flux Rayleigh number $Ra_f (= RaQ_b)$. The best-fit line suggests $Q_{top} \propto Ra_f^{0.6}$, which approximates the Nusselt number (Nu) correlation $Nu \propto Ra_f^{0.5}$ reported by Echaniz (1984). The scatter in the data points suggests some dependence on Ra as well.

The convection-dominated solutions discussed so far have the descending leg in the middle, and ascending legs at the sides. Clearly, from symmetry arguments a solution with descending legs at the sides and an ascending leg in the middle must also exist. Such solutions can be generated by using appropriate perturbations, for example a hot spot in the middle and cold spots along the sides.

3.3. *Oscillatory-convection regime*

Oscillatory convection is observed experimentally for high-permeability porous beds (i.e. high Ra). Such solutions can also be generated numerically for high Rayleigh numbers by introducing asymmetric perturbations into a one-dimensional initial conduction field. In laboratory experiments there can be several sources of asymmetric perturbations, which may explain why oscillatory convection can be triggered for high-permeability porous beds.

Oscillatory solutions for $Ra = 60$, $Q_b = 7$ and 10 are depicted in figures 11 and 12,

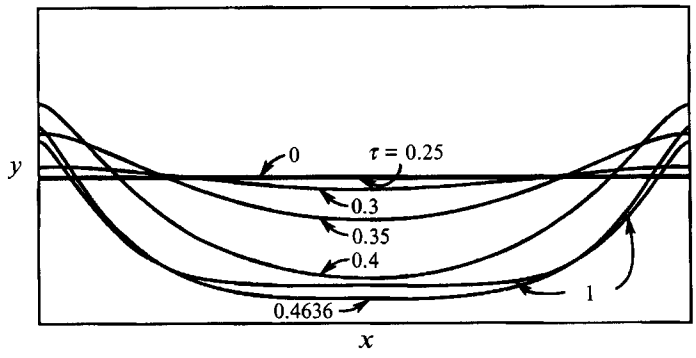

FIGURE 8. Transient interface motion for conditions corresponding to figure 6(*b*), $Ra = 50$, $Q_b = 7$. Initial condition: one-dimensional conduction solution.

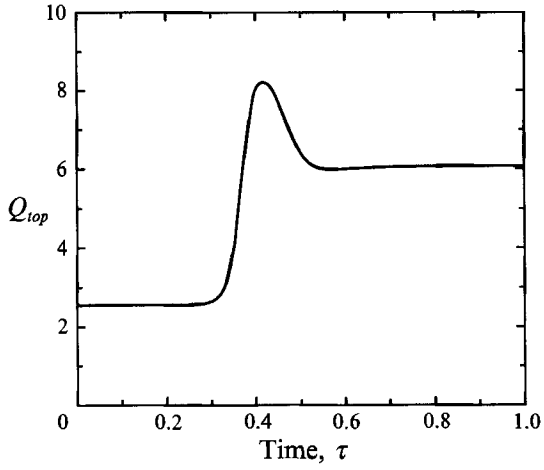

FIGURE 9. Heat transfer through the porous bed: Q_{top} versus time for conditions corresponding to figure 6(*b*), $Ra = 50$, $Q_b = 7$. Onset of convection takes place at time ≈ 0.25.

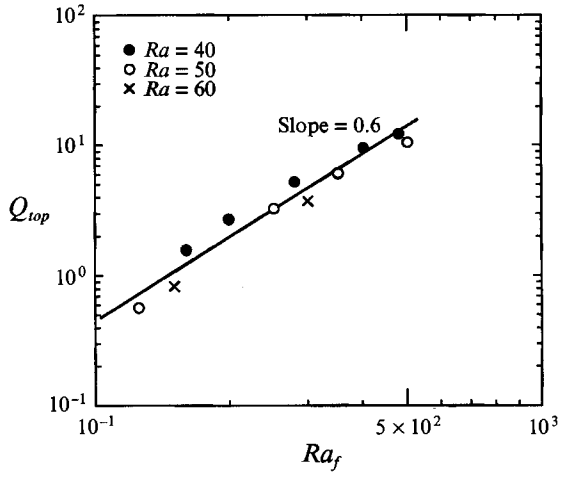

FIGURE 10. Q_{top} versus Ra_f for two-cell convection solutions. The best fit through the data points is indicated by the solid line.

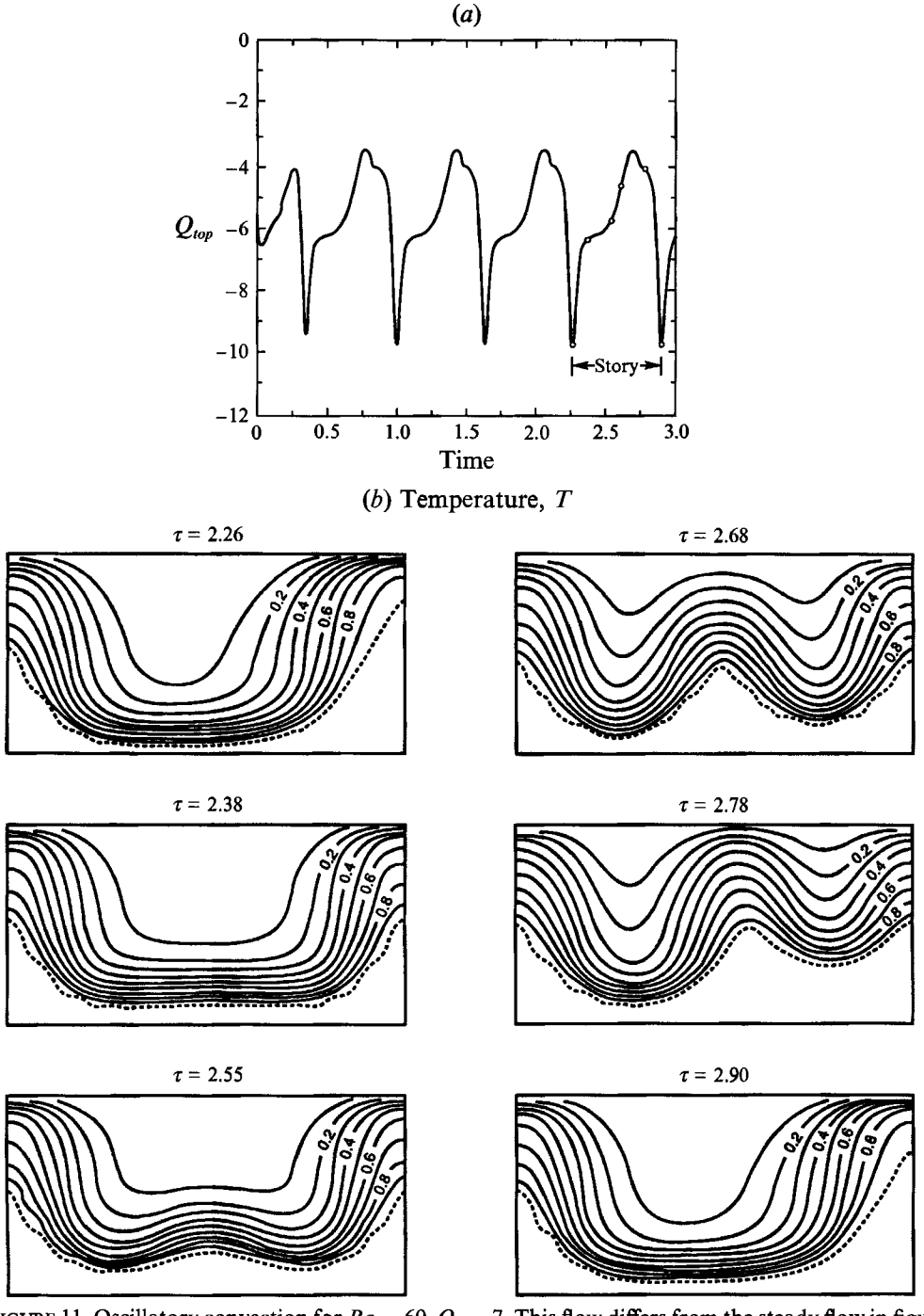

FIGURE 11. Oscillatory convection for $Ra = 60$, $Q_b = 7$. This flow differs from the steady flow in figure 7(*c*) in that it started from an asymmetric initial disturbance. Period of oscillations = 0.64. (*a*) Q_{top} versus time. (*b*) Isotherm, T, variation with time. Individual graphs correspond to the open circles in (*a*) during the time period marked 'Story'.

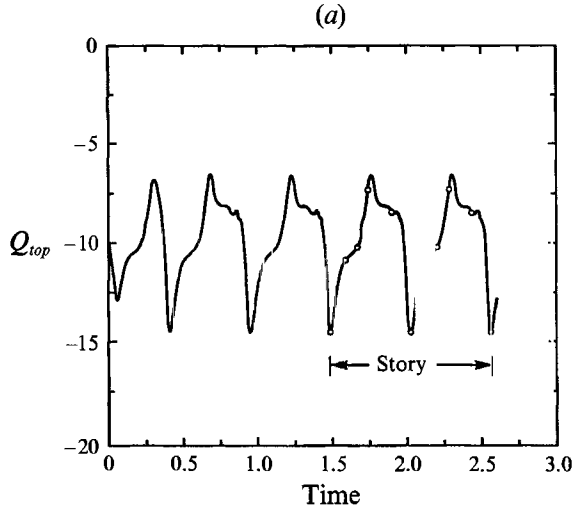

FIGURE 12(*a*). For caption see facing page.

respectively. Steady-state counterpart solutions for these two cases (using symmetric initial disturbances) are shown in figures 7(*c*) and 7(*d*). The oscillatory solutions were generated by introducing asymmetric perturbations in a one-dimensional conduction solution (a hot spot near the left sidewall) and correspond to converged limit-cycle behaviour. Figures 11(*a*) and 12(*a*) show the variation in heat transfer through the bed (Q_{top}) versus time and figures 11(*b*) and 12(*b*) show the corresponding isotherm variations during one cycle. Individual isotherm graphs correspond to the open circles shown on the heat flux transients. In figure 11(*b*), the isotherms clearly show the formation of a thermal by the distortion of the phase interface in the middle of a two-cell streamline pattern. As the thermal grows, the solution evolves to a four-cell pattern. The thermal escapes through the upper permeable boundary, and the solution returns to the two-cell pattern. The minimum heat transfer corresponds to the four-cell pattern, while the maximum heat transfer corresponds to the two-cell pattern. In figure 12(*b*), the isotherm patterns repeat every two cycles in the Q_{top} versus time curve. The thermal disappears alternately from the top left and the top right of the bed. Similar oscillations were observed in experiments (Echaniz 1984). Note the mirror symmetry of the isotherm graphs in the left and right columns of figure 12(*b*); each left–right pair corresponds to the same phase point in successive cycles of the oscillations.

The time period of the oscillations (τ_p) decreases with increase in Q_b. The time periods are of the order of hours (15 to 20 h) for the results reported here. In the experiments, the time periods varied from 3 to 10 hs. A comparison of the dependence of heat transfer rates (Q_{top}) and time period (τ_p) on Ra_f is given in table 2. It is interesting to note that the heat transfer rates are drastically increased by the onset of oscillatory convection.

The oscillatory flows in figures 11 and 12 undergo periodic transitions from a two-cell pattern to a four-cell pattern through a series of asymmetric intermediate structures. This may explain why asymmetric perturbations are required to generate oscillatory flows. Symmetric perturbations generate symmetric solutions but not the asymmetric disturbances apparently required to trigger oscillations. At low Rayleigh numbers, there is sufficient damping in the system to prevent asymmetric perturbations

(*b*) Temperature, T

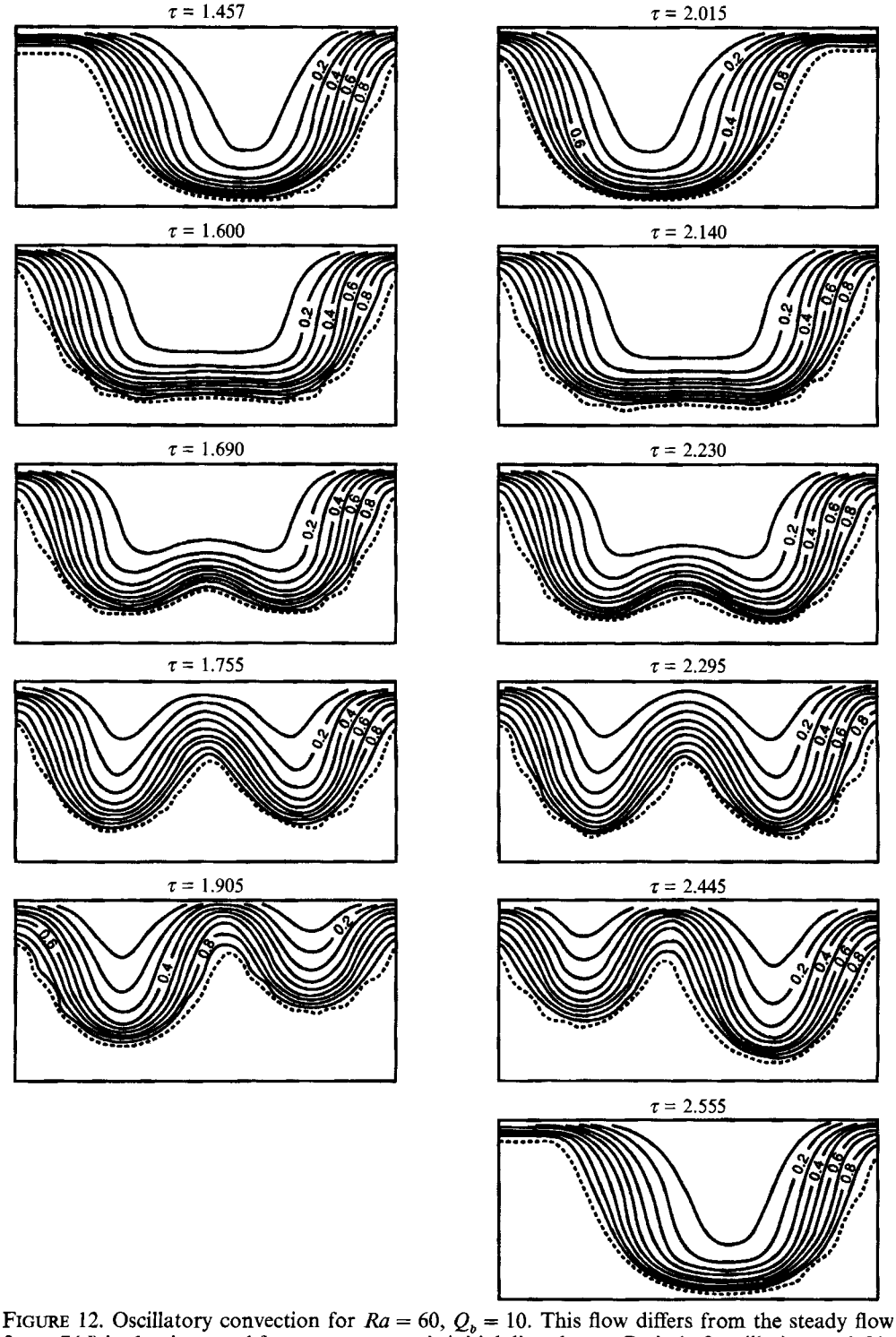

FIGURE 12. Oscillatory convection for $Ra = 60$, $Q_b = 10$. This flow differs from the steady flow in figure 7(*d*) in that it started from an asymmetric initial disturbance. Period of oscillations = 0.54. (*a*) Q_{top} versus time. (*b*) Isotherm, T, variation with time. Individual graphs correspond to the open circles in (*a*) during the time period marked 'Story'.

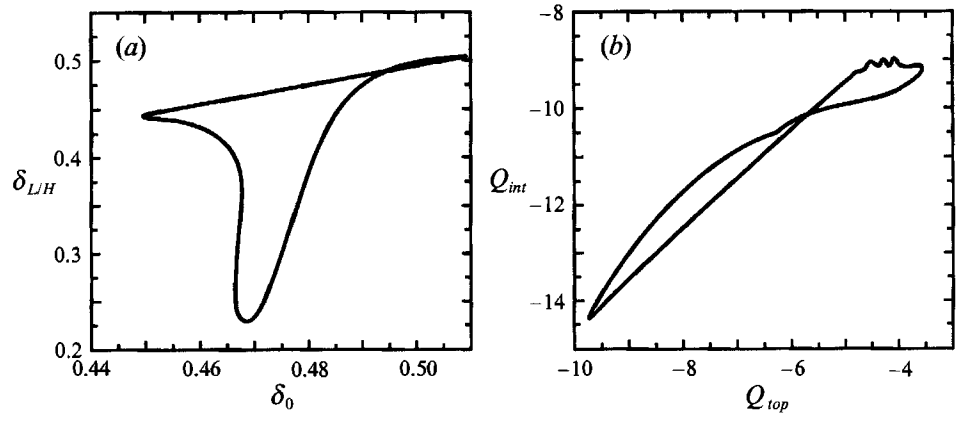

FIGURE 13. Two-dimensional phase portraits for the oscillatory flow in figure 11, $Ra = 60$, $Q_b = 7$. (*a*) Projection in δ_1–δ_M phase space. (*b*) Projection in Q_{top}–Q_{int} phase space.

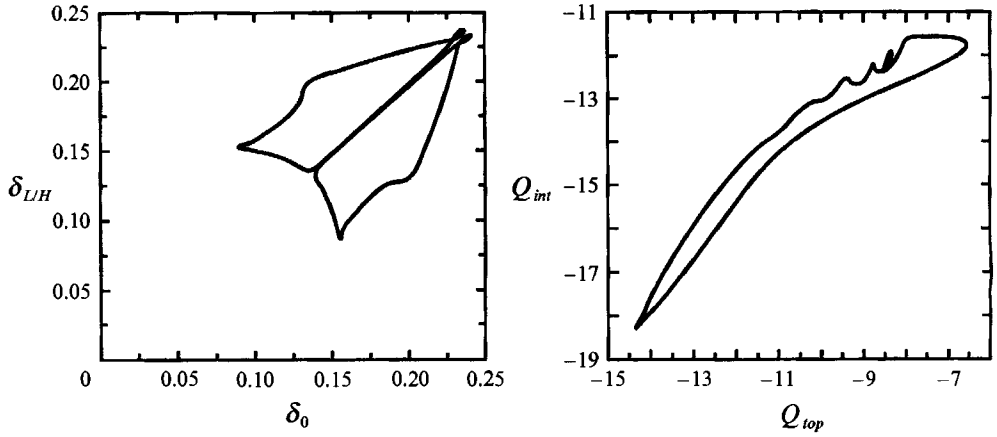

FIGURE 14. Two-dimensional phase portraits for the oscillatory flow in figure 12, $Ra = 60$, $Q_b = 10$. (*a*) Projection in δ_0–$\delta_{L/H}$ phase space. (*b*) Projection in Q_{top}–Q_{int} phase space.

from growing and consequently symmetric solutions are still preferred. However, at high Rayleigh numbers, the damping is small, and any asymmetric perturbations introduced in the solution continue to circulate within the system.

To understand time-dependent solutions in large-dimensional computational phase space, it is often useful to consider projections of the solution in a two-dimensional space. The projections may be constructed in many ways, the simplest being to use the state variable values at a few grid points. Another possible projection is to use a global variable such as the heat transfer through the porous bed. Figures 13 and 14 show two such phase projections for $Q_b = 7$ and $Q_b = 10$, respectively. The first projection is δ (interface position) at the two sides of the porous bed, denoted by δ_0 at $x = 0$ and $\delta_{L/H}$ at $x = L/H$. The second projection is the net heat transfer across the interface (Q_{int}) and the net heat transfer at the top (Q_{top}). Note that in figure 14, the global projection (Q_{int} versus Q_{top}) does not indicate the flip-flop behaviour of the thermals, whereas the local projection (δ_0 versus $\delta_{L/H}$) does. Figures 13 and 14 confirm the periodic nature of the solutions. No chaotic solutions were observed for the range of parameters considered here.

Thus, the boiling–convecting system can display either steady four-cell or oscillatory

two-cell/four-cell convection patterns at fixed values of Ra and Q_b, depending on whether symmetric or asymmetric initial disturbances are used, respectively. Further work needs to be done to verify if this is a criterion for oscillatory convection.

3.4. *Effect of initial conditions*

At high heat fluxes, steady-state solutions may also depend on the choice of initial conditions. To elaborate, consider the case $Ra = 40$, $Q_b = 12$. Linear stability theory (Ramesh & Torrance 1990*a*) suggests that the one-dimensional conduction solution is stable for this choice of parameters (see also §3.5 and figure 15 of this paper). This can indeed be verified numerically by using the one-dimensional conduction solution as the initial condition and perturbing it. But if the initial condition is instead the steady-state convective solution for $Ra = 40$, $Q_b = 10$ (figure 5*e*), then the solution converges to a two-cell convective solution. The second choice of initial condition represents a large-amplitude perturbation from the one-dimensional conduction solution and therefore cannot be predicted by linear stability theory.

3.5. *Stability boundaries in Ra–Q_b space*

Using linear stability analysis it is possible to determine the boundaries of some of the numerically observed solution regimes in Ra–Q_b parameter space. The curves in figure 15 were obtained by using the stability analysis of Ramesh & Torrance (1990*a*), with a non-zero heat-loss parameter of $Bi = 8.4$, and assuming a two-cell (wavenumber π) mode. The curves divide the solution space into four regimes, corresponding to a conductive liquid layer (region I) and a convective liquid layer (region II), both without underlying two-phase zones, and a conductive liquid layer (region III) and a convective liquid layer (region IV), both with underlying two-phase zones. Thus, in regions I and III there is no convection in the liquid layer, whereas in regions II and IV there is.

Also superimposed in figure 15 are data points from the present numerical experiments. It should be pointed out that the linear stability theory considers only the first (or leading)-order effects whereas the present study based on the numerical solution of the complete equations allows for higher-order effects as well. It is interesting to note that the linear stability analysis does predict the transitions corresponding to the onsets of convection and boiling that were obtained numerically. The sole exception is the one point for $Ra = 40$, $Q_b = 12$ for which either steady-convective or steady conductive liquid layer solutions could be obtained numerically depending on the initial condition. Such transitions, and mode switching to oscillatory flows, are not predicted by linear stability theory. Further, using finite-amplitude numerical solutions to define the transition curves would require significantly larger computational resources than were available for the present study.

Based on the numerical solutions and the linear stability analysis, the following conclusions can be drawn:

(i) Conduction solutions in regime III are unstable to large perturbations at high Rayleigh numbers.

(ii) For high Rayleigh numbers in regime IV, increasing the heat flux leads to transitions to higher-wavenumber convective solutions.

(iii) For high Rayleigh numbers and heat fluxes in regime IV, steady convective solutions may be unstable to asymmetric perturbations leading to oscillatory flows.

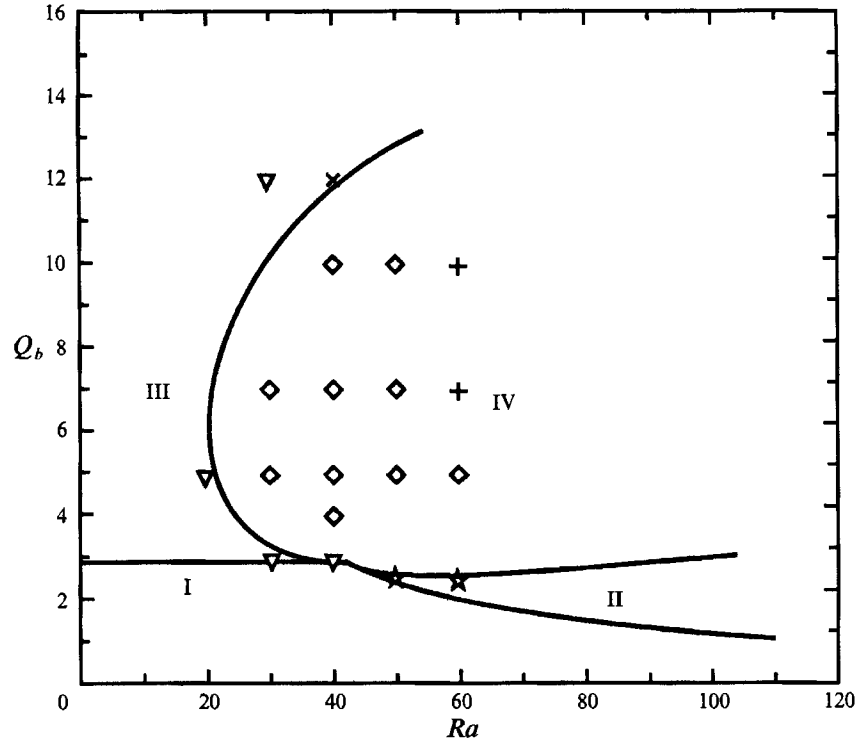

FIGURE 15. Comparison of numerical solutions (symbols) and linear stability theory (solid lines) in Ra–Q_b parameter space. I, II, III and IV denote four solution regimes: I, a conductive liquid layer – no boiling; II, a convective liquid layer – no boiling; III, a conductive liquid layer overlying a two-phase layer; IV, a convective liquid layer overlying a two-phase layer. The numerically observed solution regimes are: ★, steady convective liquid layer – no boiling; ▽, steady conductive liquid layer overlying a two-phase layer; ◇, steady convective liquid layer overlying a two-phase layer; +, steady or oscillatory convective liquid layer overlying a two-phase layer; ×, steady conductive or steady convective liquid layer overlying a two-phase layer.

4. Summary

Results of a numerical study of boiling and natural convection in a fluid-saturated porous medium, with a moving liquid/two-phase interface, are reported. The finite-amplitude solutions agree with a linear stability analysis of the system as well as with prior laboratory experiments. Transitions to multiple-cell solutions, and effects of initial conditions and perturbations, were studied. At high Rayleigh numbers, steady or oscillatory convection solutions may occur depending on whether symmetric or asymmetric perturbations trigger the convection, respectively.

This paper is based on the doctoral dissertation of the first author which was supported by the Division of Mechanical Engineering and Applied Mechanics of the National Science Foundation under Grant MEA-8401489. Computations were carried out using the Cornell National Supercomputer Facility, a resource of the Center for Theory and Simulation in Science and Engineering (Cornell Theory Center), which receives major funding from the National Science Foundation and IBM Corporation, in addition to support from New York State and members of the Corporate Research Institute.

REFERENCES

BAU, H. H. & TORRANCE, K. E. 1982*a* Boiling in low-permeability porous materials. *Intl J. Heat Mass Transfer* **25**, 45–55.

BAU, H. H. & TORRANCE, K. E. 1982*b* Thermal convection and boiling in a porous medium. *Lett. Heat Mass Transfer* **9**, 431–441.

BJORNSSON, S. & STEFANSSON, V. 1987 Heat and mass transport in geothermal reservoirs. In *Advances in Transport Phenomena in Porous Media* (ed. J. Bear & M. Y. Corapcioglu), pp. 143–183. Martinus Nijhoff.

CHENG, P. 1978 Heat transfer in geothermal systems. *Adv Heat Transfer* **14**, 1–105.

ECHANIZ, H. L. 1984 Oscillatory convection with boiling in a water-saturated porous medium. MS thesis, Cornell University.

GARY, J. & KASSOY, D. R. 1981 Computation of steady and oscillatory convection in saturated porous media. *J. Comput. Phys.* **40**, 120–142.

HORNE, R. N. & CALTAGIRONE, J. P. 1989 On the evolution of thermal disturbances during natural convection in a porous medium. *J. Fluid Mech.* **10**, 385–395.

LASSETER, T. J. 1975 The numerical simulation of heat and mass transfer in multi-dimensional two-phase geothermal reservoirs. *ASME Trans.* 75-WA/HT-71.

RAMESH, P. S. 1988 Boiling and natural convection in a fluid-saturated porous medium. PhD thesis, Cornell University.

RAMESH, P. S. & TORRANCE, K. E. 1990*a* Stability of boiling in porous media. *Intl J. Heat Mass Transfer* **33**, 1895–1908.

RAMESH, P. S. & TORRANCE, K. E. 1990*b* Numerical algorithm for problems involving boiling and natural convection in porous materials, *Numer. Heat Transfer* B **17**, 1–24.

SONDERGELD, C. H. & TURCOTTE, D. L. 1977 An experimental study of two-phase convection in a porous medium with applications to geological problems. *J. Geophys. Res.* **82**, 2045–2053.

SONDERGELD, C. H. & TURCOTTE, D. L. 1978 Flow visualization studies of two-phase thermal convection in a porous layer. *Pure Appl. Geophys.* **117**, 321–330.

TEWARI, P. K. 1982 A study of boiling and convection in a fluid-saturated porous media. MS thesis, Cornell University.

TORRANCE, K. E. 1983 Boiling in porous media. *ASME/JSME Thermal Engng Joint Conf. Proc.*, vol. 2, pp. 593–606.